J. Electrochem. Sci. Eng. **14(2)** (2024) 193-212; http://dx.doi.org/10.5599/jese.2136

Open Access : : ISSN 1847-9286
https://pub.iapchem.org/ojs/index.php/JESE

Original scientific paper

Anticorrosive characteristics of imidazole derivative on carbon steel in 1 M HCl

Asma Barrahi[1], Mohamed El Faydy[2], Loubna Adlani[3], Fouad Benhiba[1,4], Danil R. Bazanov[5], Natalia A. Lozinskaya[5], Mohamed Maatallah[6], Ismail Warad[7], Burak Dikici[8], Abdelkbir Bellaouchou[1], Abdelkader Zarrouk[1,✉]

[1]*Laboratory of Materials, Nanotechnology and Environment, Faculty of Sciences, Mohammed V University in Rabat, P.O. Box. 1014, Rabat, Morocco*
[2]*Laboratory of Organic Chemistry, Inorganic, Electrochemistry, and Environment, Faculty of Sciences, Ibn Tofaïl University, PO Box 133, 14000, Kenitra, Morocco*
[3]*Laboratory of Advanced Materials and Process Engineering, Faculty of Sciences, Ibn Tofail University, P.O. Box. 133, 14000 Kenitra, Morocco*
[4]*Higher Institute of Nursing Professions and Health Techniques of Agadir Annex Guelmim, Morocco*
[5]*Department of Chemistry, Lomonosov Moscow State University, 119991 Moscow, Russia*
[6]*Laboratory of Molecular Chemistry, Faculty of Sciences Semlalia, Cadi Ayyad University, PO Box 2390, Marrakech, Morocco*
[7]*Department of Chemistry, AN-Najah National University, P.O. Box 7, Nablus, Palestine*
[8]*Ataturk University, Department of Mechanical Engineering, 25240 Erzurum, Turkey*

Corresponding author: ✉azarrouk@gmail.com

Received: October 17, 2023; Accepted: February 21, 2024; Published: April 2, 2024

Abstract

The novelty of the work is to scrutinize for the first time the 4R,5S- 2,4,5-tris(4-ethoxy-phenyl)-4,5-dihydro-1H-imidazole (TEPI) as a corrosion inhibitor for carbon steel (C35E) in the acidic medium. The inhibitory properties of TEPI were assessed through various methods, including electrochemical, spectroscopic, and surface analysis, as well as quantum chemical calculations. The protective effect of C35E was seen to expand as the TEPI amount was extended but to diminish as temperature was augmented, fulfilling 98.3 % at 1 mM under 303 K. Certain thermodynamic and kinetic indices were estimated and explored. The TEPI complied with the Langmuir adsorption isotherm when it adsorbs on the C35E surface. TEPI behaviour was revealed by polarization trials to be of mixed type. The establishment of an adsorption-linked preventive TEPI layer on the C35E surface has been disclosed thanks to surface analysis. The outcomes of scanning electron microscopy coupled with energy dispersive X-ray spectroscopy clearly illustrate that TEPI can efficiently adsorb at the C35E interface, substantially reducing C35E steel corrosion. UV-visible analysis of the inhibited electrolyte clearly reveals the complexation of iron cations with TEPI molecules. The density functional theory (DFT), Monte Carlo(MC) and

molecular dynamic simulation (MDS) were adopted to check out the adsorption characteristics of the TEPI onto C35E surface. The laboratory outcomes have been proven by DFT and MDS.

Keywords
Corrosion inhibition; C35E steel; electrochemical methods; surface analysis; quantum chemistry calculations

Introduction

Corrosion is an electrochemical process that occurs between metallic materials and the environment, resulting in metal dissolution, process contamination, environmental damage, and economic losses [1,2]. Corrosion impacts a wide range of materials, from integrated circuits to reinforced concrete bridges. Metallic materials, and especially carbon steel, which are the primary building blocks for many structures, are highly susceptible to corrosion when they come into contact with moist environments, are submerged in fresh or salt water, or are in the presence of more or less corrosive solutions [3,4]. The assistance life of supported concrete structures has been extended by the development of numerous innovative materials and technologies. These methods, such as chloride extraction, cathodic protection, protective coatings and sealants, significant re-legalization, and corrosion inhibitor pinnacles, can prevent and reduce steel consumption in concrete.

One of the most efficacious, beneficial, dynamic, and financially rewarding strategies for preventing metal rust is the benefit of organic inhibitors [5,6]. Organic substances with heteroatoms of oxygen, nitrogen, and sulfur often enclose the ability to prevent rusting [7-12]. Organic compounds possess unshared electrons in bonds of π and heteroatoms that can be readily given to a metal vacant d orbital, rendering them effective inhibitors.

Imidazole and its derivatives are extensively used in the treatment of bacterial, viral, inflammatory, and cancerous conditions [13,14]. Furthermore, it has been proven that imidazole possesses outstanding corrosion inhibition capabilities for concrete structures. It may function as a corrosion inhibitor to stop environmental corrosion of carbon steel since it contains nitrogen atoms in the imidazole ring and conjugated π-electron system [15,16].

The primary novelty of our study lies in scrutinizing the performance of new imidazole derivatives, namely (4R,5S)-2,4,5-tris(4-ethoxyphenyl)-4,5-dihydro-1H-imidazole (TEPI), that was utilized as an organic inhibitor in acidic medium. To assess the performance of TEPI as an inhibitor and the corrosion rate of C35E, electrochemical methods were used. The C35E surface and its corrosive medium were scrutinized through the combination of scanning electron microscopy (SEM), energy dispersive X-ray spectroscopy (EDX), and UV-vis spectroscopy, respectively. Furthermore, theoretical calculations based on density functional theory (DFT), Monte Carlo (MC), and molecular dynamic (MD) simulation were used to back up the experimental findings.

Experimental

Materials

The material that operated as the working electrode in electrochemical measurements is carbon steel (C35E), and its weight and chemical composition are offered in Table 1. The surface area of C35E samples serving as electrodes was 1 cm^2. After polishing the electrode surface with various grades of Sic paper and prior to being desiccated at ambient temperature, the samples were scoured with distilled water.

By diluting hydrochloric acid of 37 % with distilled water, a corrosive medium of 1M HCl was produced. The concentration range of TEPI was 1 mM to 1000 nM, while its molecular structure is shown in Figure 1.

Table 1. *Chemical composition and element weights of carbon steel C35E*

Element	C	Fe	Ti	Co	S	Ni	Si	Mn	Cr	Cu
Content, wt.%	0.370	Balance	0.011	0.009	0.016	0.059	0.230	0.680	0.077	0.160

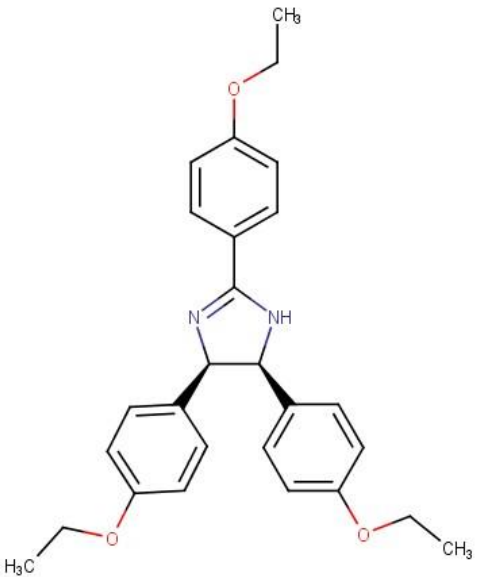

Figure 1. *Molecular structure of 4R,5S)-2,4,5-tris(4-ethoxyphenyl)-4,5-dihydro-1H-imidazole (TEPI)*

Electrochemical measurements

The 3-electrode cell was adopted for the electrochemical exams, with a saturated calomel serving as the reference electrode (SCE), a platinum wire as the auxiliary electrode, and C35E as the working electrode with an area of 1 cm^2. The C35E electrode was first immersed in the test medium for 1800 s to obtain a reliable, steady-state value of open circuit potential (E_{ocp}). After measuring the open circuit potentials, the electrochemical exams took place. The electrochemical impedance spectroscopy (EIS) was conducted at E_{ocp}, in the frequency range between 100 kHz and 10 mHz, and *ac* amplitude of 10 mV peak-to-peak, using 10 points per frequency decade. EIS diagrams were simulated using Z-view. Then, potentiodynamic polarization (PDP) was enrolled at the potential of -800 to -100 mV at a sweep speed of 0.5 mV s^{-1}. Inhibition performances (η / %) taken from EIS and PDP were determined using equations (1) and (2).

$$\eta_{pp} = \left(\frac{i_{corr°} - i_{corr1}}{i_{corr°}} \right) 100 \quad (1)$$

where $i_{corr°}$ and i_{corr1} denote the corrosion current densities before and after TEPI addition.

$$\eta_{EIS} = \left(\frac{R_{p1} - R_{p0}}{R_{p1}} \right) 100 = 100\,\theta \quad (2)$$

where R_{p1} and R_{p0} denote the polarization resistances prior and after TEPI addition, respectively, while θ is the surface coverage degree.

For the uninhibited solution, data from electrochemical measurements were taken from our previously published study [17]. This decision was made as the experiments were conducted under identical conditions and with the same equipment.

Ultraviolet-visible spectroscopy

To better comprehend how the TEPI interacts with the C35E surface in an aggressive medium, as well as the development of iron-TEPI complexes, the inhibited and uninhibited solutions of 1.0 M HCl were subjected to UV-visible spectroscopy employing a JASCO V-700 UV-Visible spectrophotometer before, and after 3 days of C35E submersion.

Combination of scanning electron microscopy and energy dispersive X-ray

The surface morphologies of C35E exposed to 1M HCl medium without and with 0.001M of TEPI for 24 hours at 303 K were investigated by SEM. It normally operates with an EDX unit and an acceleration voltage of 20 kV. SEM results obtained in the absence of the inhibitor were taken from the work already published by our research team [18].

Calculations involving quantum chemistry

Theoretical studies utilizing density functional theory were executed to better apprehend the association among the molecular characteristics of TEPI and their inhibition effectiveness [18,19]. The computation was carried out through the Gaussian 09 prog. package [20] and the DFT technique with the B3LYP functional and 6-31G (d, p) and 6-311G (d, p) basis sets [21-24]. The theoretical descriptors such as the energy of the highest occupied (E_{HOMO}), unoccupied molecular orbital (E_{LUMO}), energy gap (ΔE), electron transferred fractions (ΔN), chemical hardness (η), electronegativity (χ), dipole moment (μ), and polarizability (α) were determined by the application of equations cited in past studies [25,26].

Monte Carlo and molecular dynamic simulations

Materials Studio 8 software was used to evaluate the TEPI adsorption processes on the C35E surface. The Fe (110) surface simulation was carried out by putting the surface crystal in a cell measuring 2.73×2.70×3.71 nm^3 using a 6-couche slab model for each layer, making up an (11×11) unit cell. The liquid phase was made up of 500 H_2O, $5Cl^-$, and $5H_3O^+$. On top of the liquid layer, a 40- vacuum layer was created to prevent interaction between the surface and periodic repeating planes. The simulations were carried out at 303 K under NVT ensemble control using an Andersen thermostat. The simulation was performed by Forcite code in a COMPASS force field for 1000 ps with a time step of 0.1 fs. The diffusion of Cl^-, H_3O^+, and H_2O in inhibitor membranes was also simulated [27,28].

Results and discussion

The polarization curves

Figure 2 depicts the polarization graphs at 303 K prior and after multiple amounts of TEPI added in the 1 M HCl medium. Table 2 supplies details on the relevant extrapolated electrochemical indices, such as corrosion potential (E_{corr}), corrosion current (i_{corr}), and cathodic and anodic Tafel slopes (β_c and β_a). A preliminary analysis of Tafel branches revealed that adding TEPI to the acidic environment lessens both anodic and cathodic current densities, implying that the presence of TEPI limits both C35E dissolving and cathodic hydrogen evolution. Furthermore, it is evident that the inhibitory effect of TEPI on the reduction of hydrogen (H^+) is considerably greater than on the C35E dissolution reaction. It is also noted that the cathodic segments of the polarization current potential curves result in Tafel lines that are nearly parallel. This phenomenon reveals that the process of hydrogen evolution remains unchanged with the addition of TEPI. Most likely, the reduction of

hydrogen ions on the C35E surface takes place mostly through a charge transfer mechanism [29]. In this manner, the surface area available for H^+ ions became reduced while the actual reaction mechanism remains unaltered. Table 2 clarifies that TEPI amounts have a small effect on β_c but a big impact on β_a. Also, the β_a deviations display that TEPI affects the anodic process kinetics. The practically constant values of β_c for TEPI suggest that it was initially adsorbed onto the C35E surface and hindered by simply obstructing the C3E active sites without changing the cathodic mechanism. The E_{corr} value moved in the positive direction after the TEPI was added, and its shift is less than 27.66 mV, inferring that the TEPI performs as a mixed-type corrosion inhibitor [30]. However, as the amount of TEPI rises, the i_{corr} decreases, which could be owing to the TEPI adsorbing on the C35E surface. The inhibition efficiency rose with the TEPI amount, getting 97.7 % at 1 mM imidazole. TEPI offers high performance relative to the imidazoles mentioned in the literature, and this is due to the molecule's high electron densities provoked by the existence of π-electrons in the imidazole and ethoxy phenyl rings and lone pair electrons in nitrogen atoms.

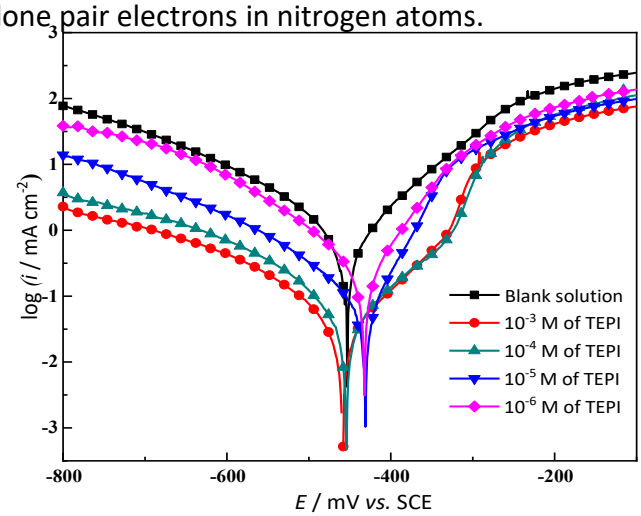

Figure 2. *PDP segments for C35E corrosion in 1 M HCl ahead of and after TEPI addition*

Table 2. *Extrapolated indices for C35E corrosion in 1 M HCl prior and after TEPI addition*

Medium	*C* / μM	-E_{corr} / mV *vs.* SCE	i_{corr} / μA cm^{-2}	Tafel slopes, mV dec^{-1}		η_{pp} / %
				-β_c	β_a	
Blank	---	456.3	1104	112	155.4	---
TEPI	1000	457.77	24.61	98.0	83.2	97.7
	100	453.64	38.15	94.0	97.7	96.5
	10	428.64	60.15	98.7	48.3	94.6
	1	431.45	140.53	77.7	50.9	87.3

Electrochemical impedance spectroscopy

The corrosion behavior of C35E in the acidic medium prior and after TEPI addition was investigated by electrochemical impedance spectroscopy (EIS), and its outcomes are displayed in Figure 3. All collected impedance spectra display simply one depressed half-circle bonded to charge transfer during the corrosion process [31], and their size improves with rising TEPI concentration. The impedance loops in Nyquist plots do not produce perfect half-circles, typically ascribed to the roughness of the metal interface and/or frequency dispersion [32]. Comparable capacitive loops might illustrate that, in the lack or presence of TEPI, the charge transfer mechanism controls the electrode reactions. The capacitive loop clearly grows when TEPI is present, showing a strong inhibiting impact of TEPI. A single-phase angle peak can be seen in the Bode graphs (Figure 4), implying a single time constant. The peak amplitude at intermediate frequency becomes more extensive as the concentration of TEPI increases, indicating the adsorption of more TEPI molecules

on the C35E steel surface. This leads to a reduced metal dissolution rate [33]. To derive the EIS information, the EIS spectra were simulated by applying the equivalent circuit portrayed in Figure 3, and the acquired information is tabulated in Table 4. In this circuit, R_s stands for the resistance of the electrolyte solution, CPE denotes the constant phase element characterizing the double-layer capacitance (C_{dl}), while R_p stands for the polarization resistance. To suit the EIS half-circles, CPE has been swapped for C_{dl} [34]:

$$Z_{CPE} = A^{-1} (i\omega)^{-n} \quad (3)$$

where A denotes the coefficient of CPE, n denotes the exponent of CPE (dependent on a degree of surface roughness), i denotes the imaginary unit and ω the angular frequency. As a result, C_{dl} is determined by employing the formula below [34]:

$$C_{dl} = (A\ R_p^{1-n})^{1/n} \quad (4)$$

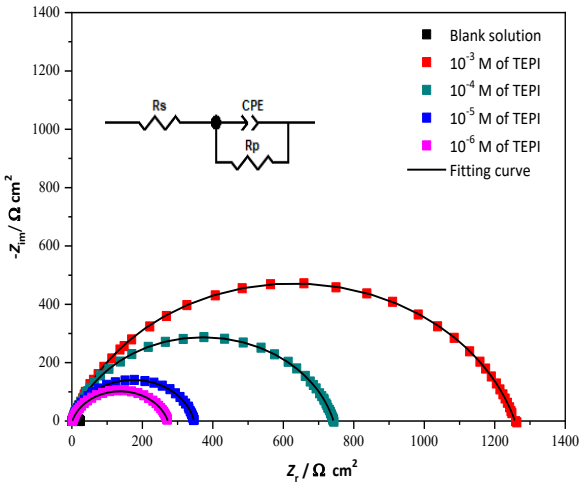

Figure 3. *Nyquist plots of C35E corrosion in 1 M HCl prior and after TEPI addition*

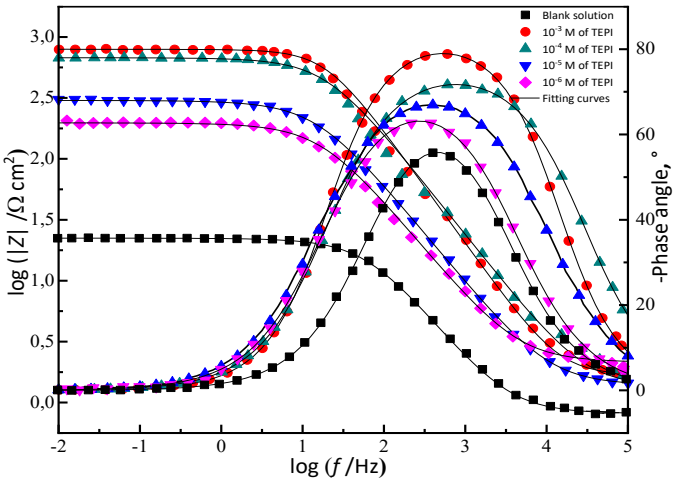

Figure 4. *Bode plots for C35E corrosion in 1 M HCl prior and after TEPI addition*

Table 3 displays that χ^2 (Chi-square is the fitting precision) was close to 0.001, offering that this model provided an outstanding match for the EIS spectra. The R_p values expand with increasing TEPI amounts, whereas the C_{dl} values reflect an opposite trend, which might result from greater coverage on the C35 surface by TEPI adsorption, leading to improved inhibition performance. The diminution in C_{dl} implies a decline of the local dielectric constant and/or growth in the thickness of the electrical double layer, implying that the TEPI molecules perform *via* adsorption on the C35E/solution interface [35]. Furthermore, the readings of n in the presence of TEPI were higher than in the absence of TEPI, signifying growth in the homogeneity of the C35E surface with adsorbed inhibitor [30]. It is clear that the inhibition effectiveness was inhibitor amount dependent, reaching 98.3 % at 0.001 M, proving that TEPI is a potent corrosion inhibitor for C35 in the acidic medium.

Table 3. *EIS factors for C35E corrosion in 1 M HCl prior and after TEPI addition*

	C / μM	R_s / Ω cm^2	R_p / Ω cm^2	C_{dl} / μF cm^{-2}	A / μΩ^{-1} s^n cm^{-2}	n	χ^2	η_{EIS} / %	θ
Blank	0	0.83	21.57	116.2	293.9	0.845	0.002	-	-
TEPI	1000	1.16	1256.0	10.5	22.9	0.880	0.006	98.3	0.983
	100	1.64	741.0	13.7	28.5	0.868	0.009	97.1	0.971
	10	1.82	344.0	33.7	60.2	0.860	0.008	93.7	0.937
	1	1.20	271.0	35.5	81.6	0.859	0.009	92.1	0.921

Temperature influence and activation factors

The temperature has a powerful impact on corrosion rate and inhibitor performance, particularly in acidic medium. Corrosion happens more quickly as the temperature increases. The performance of inhibition of TEPI was investigated at various temperatures varying from 303 to 333 K prior and after the addition of 0.001 M TEPI for examining the mechanism of inhibition and estimating activation factors of the corrosion process by exploiting PDP experimentations presented in Figure 5. The related electrochemical indices are gathered in Table 4.

Figure 5 and data in Table 4 demonstrate that the growth in i_{corr} becomes apparent when the temperature augments prior and after the addition of TEPI and that the improvement in the uninhibited solution is more noticeable when compared to the rise in the inhibited solution, meaning that the temperature rise slows the process of adsorption of TEPI molecules on the C35E surface. The effectiveness only dropped by 5.1 % when TEPI was present in the temperature range, demonstrating the potent inhibitory power of TEPI and its independence from temperature [35].

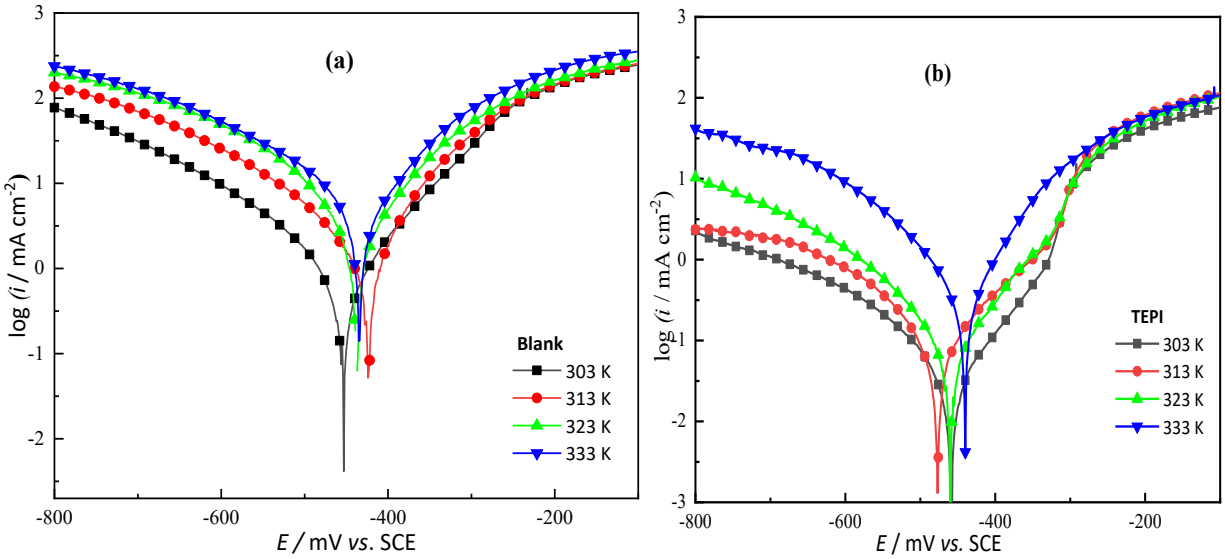

Figure 5. *PDP segments for C35E corrosion in 1 M HCl without (a) and with 1 mM of TEPI (b) under temperatures varying from 303 to 333 K*

Table 4. *PDP factors for C35E corrosion in 1 M HCl without and with 1 mM of TEPI under temperatures varying from 303 to 333 K*

Medium	T / K	$-E_{corr}$ / mV *vs.* SCE	i_{corr} / µA cm^{-2}	Tafel slopes, mV dec^{-1}		η_{pp} / %
				$-\beta_c$	β_a	
Blank	303	456.3	1104	112	155.4	---
	313	423.5	1477.4	131.3	91.3	-
	323	436.3	2254.0	117.8	91.4	-
	333	433.3	3944.9	134.6	103.9	-
TEPI	303	457.8	24.6	98.0	83.2	97.8
	313	475.5	62.4	100.2	93.3	95.8
	323	441.8	129.6	94.9	90.9	94.2
	333	436.1	287.5	93.1	66.4	92.7

The information on temperature influence was exploited to determine the activation kinetic parameters through Arrhenius and the transition-state relationships, Equations (5) and (6):

$$i_{corr} = A e^{\left(\frac{-E_a}{RT}\right)} \quad (5)$$

$$i_{corr} = \frac{RT}{Nh} e^{\left(\frac{\Delta S_a}{R}\right)} e^{\left(\frac{-\Delta H_a}{RT}\right)} \quad (6)$$

where A denotes the Arrhenius pre-exponential factor, T is temperature, R is the universal gas constant, h denotes the Planck's constant, N denotes the Avogadro number, E_a symbolizes the energy of apparent activation, ΔH_a denotes the enthalpy, and ΔS_a denotes the entropy of apparent activation.

The magnitudes of E_a, ΔS_a, and ΔH_a listed in Table 5 were determined from the slope of Arrhenius plots (Figure 6a) and the intercept and slope of the transition state plots (Figure 6b), respectively.

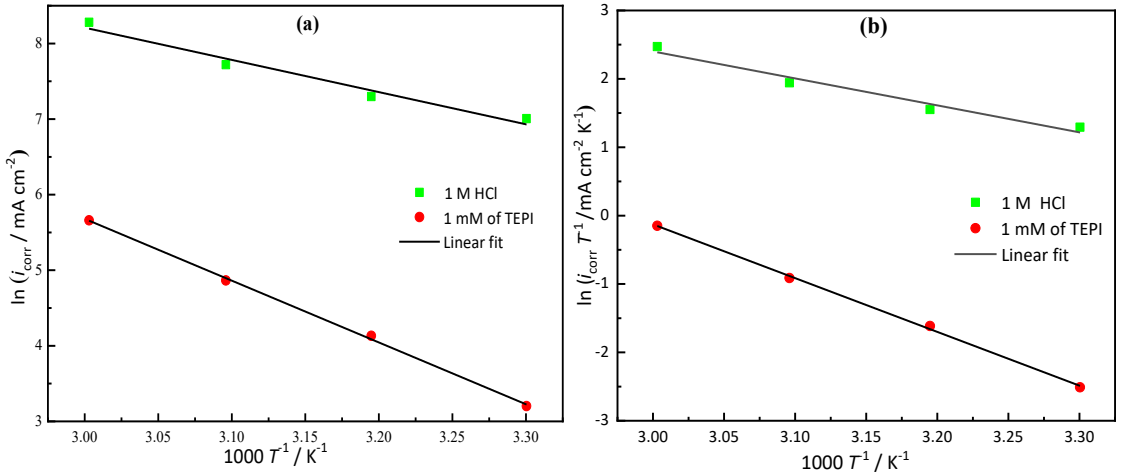

Figure 6. *Arrhenius (a) and transition-state (b) plots for C35E dissolution in 1 M HCl prior and after addition of 1 mM TEPI*

Inspection of Table 5 shows that the magnitude of E_a is augmented when TEPI is present, strongly pointing out that TEPI molecules are fixed to the C35E surface through physical adsorption (electrostatic interactions) [36]. The corresponding magnitude of ΔH_a for TEPI is higher than in its absence, suggesting that the dissolution of C35E becomes slower in the presence of TEPI. Furthermore, the magnitudes of ΔH_a are both positive and reflect the endothermic character of the C35E dissolution process [37,38]. Related magnitudes of ΔS_a for TEPI were negative in its absence or presence in the medium. Besides, the magnitude of ΔS_a for TEPI is higher than in its absence, exhibiting a rise in the disorder during the transformation of the reactants into activated complexes.

Table 5. E$_a$, ΔH$_a$ *and* ΔS$_a$ *values for C35E dissolution in 1 M HCl prior and after the addition of 1 mM TEPI*

	E_a / kJ mol^{-1}	ΔH_a / kJ mol^{-1}	ΔS_a / J mol^{-1} K^{-1}
Blank	35.4	32.7	-79.2
TEPI	67.9	65.3	-2.5

Adsorption isotherm

The thermodynamic details of the adsorption process assist in comprehending the inhibition mechanism for an inhibitor on the metal surface. Physical and chemical adsorption are two main kinds of interactions that may characterize molecular adsorption [39]. In this context, the surface coverage values (θ) (defined by Eq. (2)) for different TEPI concentrations can be calculated from the EIS data (Table 3) to present the best adsorption isotherm. Multiple attempts have been undertaken to fit the θ values to adsorption isotherms, including Langmuir, Temkin, and Frumkin, as illustrated in Figure 7. The correlation coefficient (R^2) values and the slopes of the straight lines depicted in Figure 7 remain relatively close to unity for Temkin and Frumkin. At the same time, for Langmuir,

they are equal to unity. Therefore, the Langmuir adsorption isotherm demonstrates the best potential adsorption model of the TEPI molecules onto the C35E surface in the acidic medium, which may be formulated in linear terms as follows [32]:

$$\frac{C}{\theta} = \frac{1}{K_{ads}} + C \quad (7)$$

where K_{ads} denotes the adsorption equilibrium constant.

Equation (8) links K_{ads} value to Gibbs free energy ΔG_{ads}^0 [32]:

$$\Delta G_{ads}^0 = -RT \ln (55.5\ K_{ads}) \quad (8)$$

where R denotes the constant of universal gas and 55.55 stands for H_2O concentration.

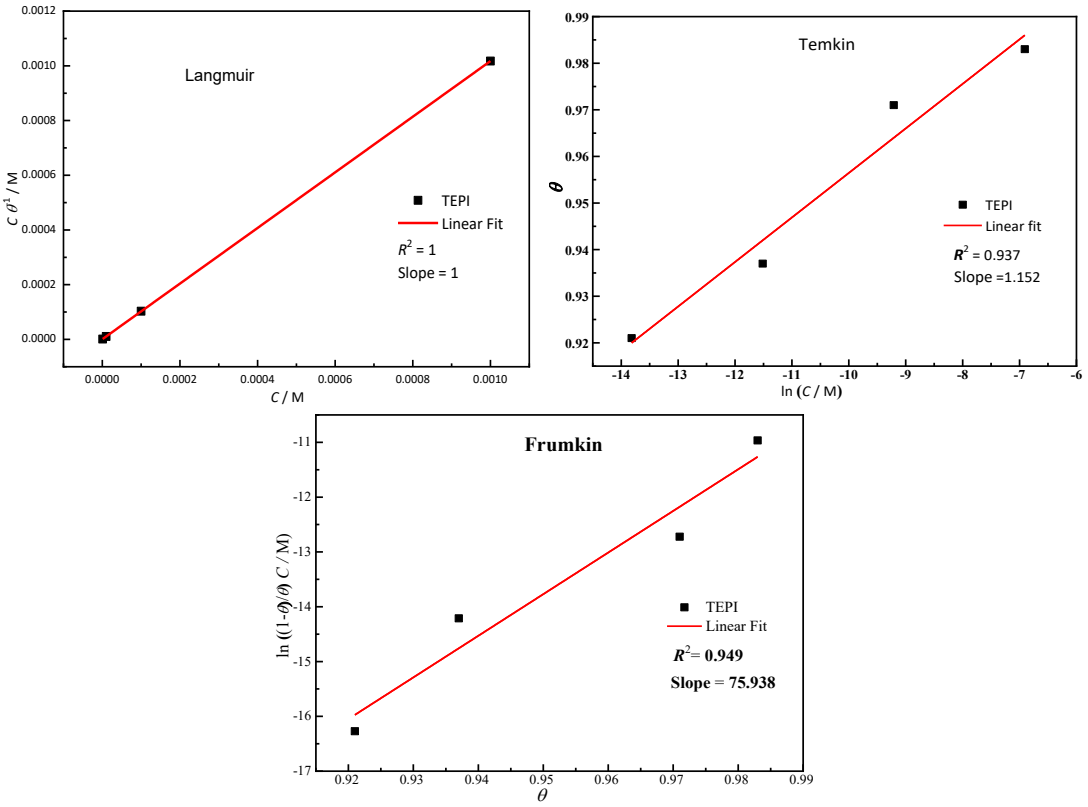

***Figure 7**. Various isotherm models for C35E in 1 M HCl with 1 mM TEPI at 303 K*

The values of ΔG_{ads}^0 and K_{ads} are listed in Table 6. The high magnitude of K_{ads} demonstrates that TEPI molecules adsorb powerfully on the C35E surface [39]. The ΔG_{ads}^0 value means the TEPI molecules are chemisorbed at the C35E surface [40]. The TEPI molecules contributing lone electron pairs and/or electrons and Fe empty orbitals work together to form chemical bonds with Fe unfilled orbitals.

***Table 6.** K_{ads} and ΔG_{ads}^0 for TEPI adsorption*

	K_{ads} / M^{-1}	ΔG_{ads}^0 / kJ mol^{-1}	Slope	R^2
TEPI	1.652×10^6	-46.2	1	1

UV-visible spectroscopy

The complexation process between Fe ions and the inhibiting molecules can be utilized to investigate the underlying mechanism of anticorrosion prevention of carbon steel since Fe is an essential element of C35E. The earlier study, however, revealed that a modification in wavelength with the increase or decrease in absorbance implies the development of a complex involving Fe and molecules present in the corrosive medium [41]. The UV-visible spectrum of TEPI in the acidic

medium prior to C35E submerging showed two absorption bands at 210 and 273 nm because of an n-π* and π-π* electronic transitions, resulting from the heteroatoms lone pair on the pyridine ring (Figure 8). After 3 days of C35E submerging, the bands appeared to have shifted blue (the first to 207 nm and the second to 255 nm), with a rise in absorbance. These modifications occurred probably due to the formation of complexes among Fe^{2+} ions and TEPI species in the acidic medium.

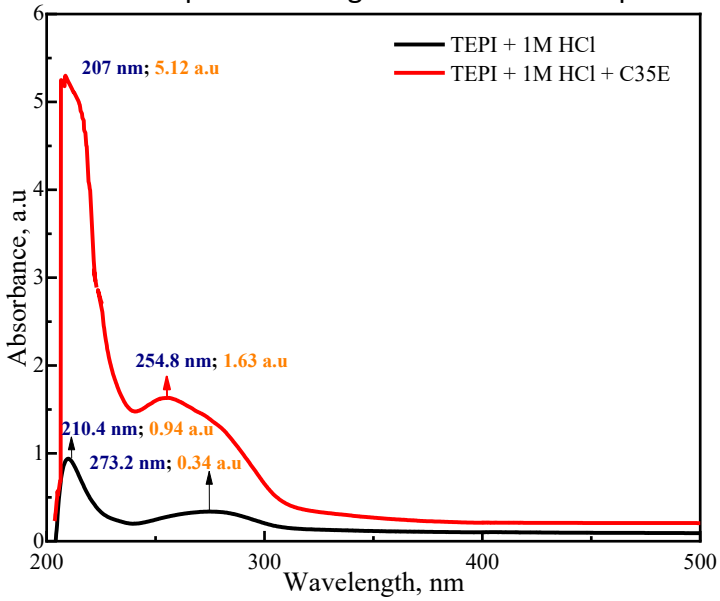

Figure 8. *UV-visible absorption spectra of 1 M HCl containing 0.001M of TEPI prior and after C35E dipping*

SEM/EDX analysis

Figure 9 shows the scanning electron micrographs of C35E samples prior and after 24 h of soaking in 1 M HCl, without and with 1 mM of TEPI at 303 K. Figure 9a1 displays the polished steel sample without flaws other than polishing scratches. In Figure 9b1, the specimen surface was poorly harmed, with profound holes indicating severe corrosion. When TEPI was added to the 1 M HCl medium, the C35E surface area exhibited a few small pinholes and low damage (Figure 9c1), demonstrating its strong ability to reject corrosive ions. This ability generally results from TEPI adsorption on the C35E surface by developing a protective and compact film.

The EDX spectra presented in Figures 9a2-c2 show characteristic peaks of prevailing elements such as Fe, C, Mn and Cr, constituting C35E samples (*cf*. Table 1). Also, the presence of oxides visible through the O peak is prominent for C35 samples left in 1.0 M HCl, without and with the presence of 1 mM TEPI inhibitor.

Table 7 summarizes all EDX results presented as wt.% and at.% of identified elements of C35E samples before and after 24 hours of immersion in 1.0 M HCl, without and with 1 mM TEPI. It appears that the at.% of chlorine ions in the absence of TEPI is 46.30 %, whereas it decreases to 0.38 % in its presence. The reduction of Cl^- ions in the presence of TEPI suggests that this inhibitor can be deposited on the C35E surface, protecting against attack by Cl^- ions. The percentage of atomic content of iron (Fe) for C35E immersed in the 1M HCl is 46 %. However, when C35E was dipped in the optimal concentration (1 mM) of TEPI, it increased to 83.29 %. This increase suggests that the presence of TEPI hinders the dissolution reaction of C35E in the acidic solution. Additionally, the percentage atomic content of oxygen (O) significantly decreased from 46.30 to 33.66 %. Conversely, the percentages for nitrogen (N) show a notable increase from 0 to 3.76 % in the presence of TEPI. These findings confirm the presence and formation of a protective film of TEPI on the C35E surface in 1 M HCl.

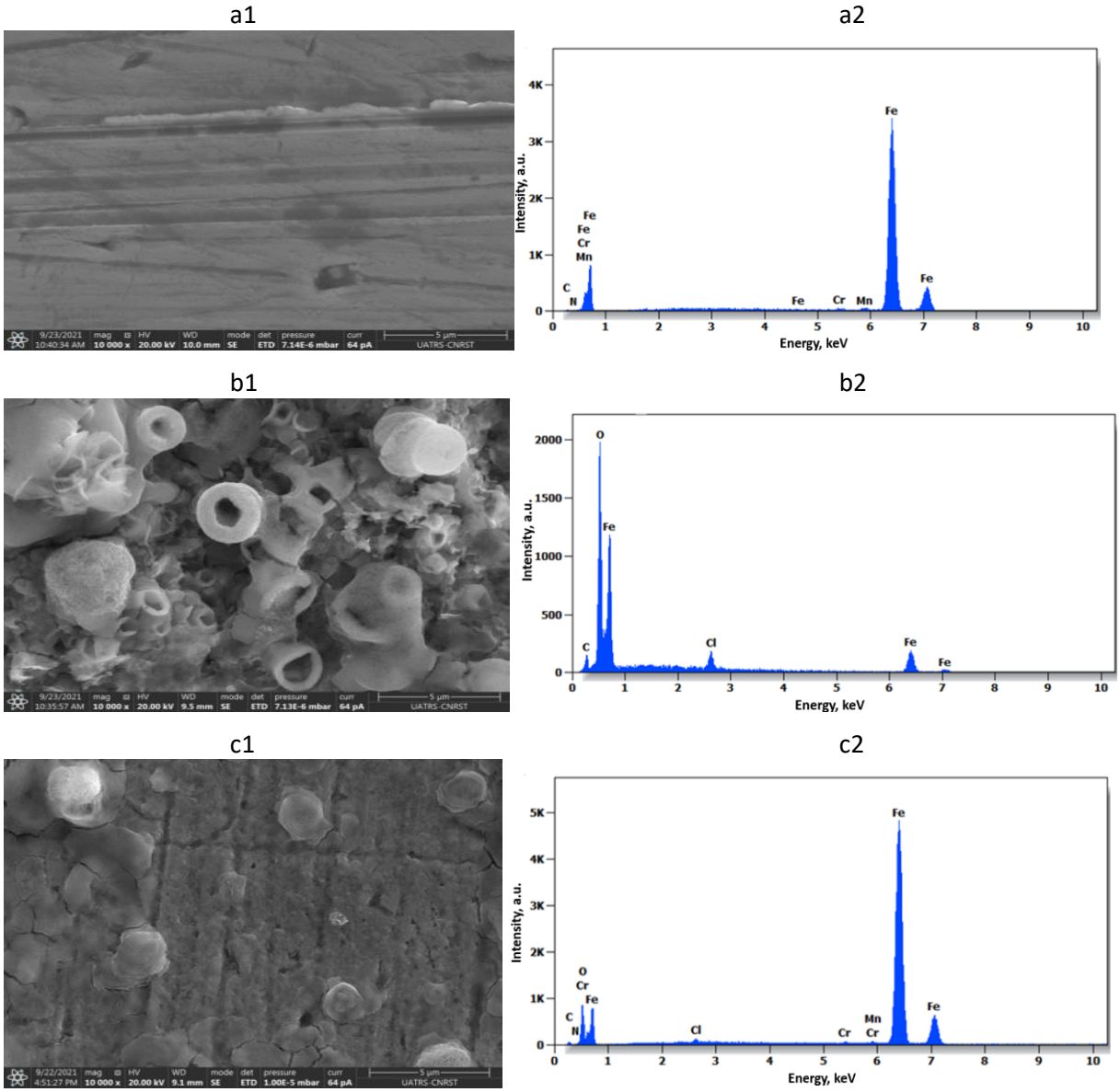

Figure 9. *SEM/EDX for C35E prior (a) and after 24 hours of soaking in 1 M HCl (b) and with 1 mM of TEPI (c) at 303 K (a1) and (b1) images are taken from [18].*

Table 7. *Percentages of atomic and weight contents of elements of C35E surface in the absence and presence of 0.001M TEPI obtained from EDX spectra*

Element	C35E (a2)		1 M HCl (b2)		TEPI (c2)	
	Content, wt.%	Content, at.%	Content, wt.%	Content, at.%	Content, wt.%	Content, at.%
C	1.43	6.17	1.40	4.05	2.66	8.24
N	0.81	3.01	-	-	1.42	3.76
O	-	-	21.24	46.30	14.49	33.66
Cl	-	-	3.70	3.64	0.37	0.38
Cr	0.33	0.33	-	-	0.30	0.22
Mn	0.77	0.73	-	-	0.66	0.45
Fe	96.66	89.76	73.66	46.00	80.09	53.29
Total	100.00	100.00	100.00	100.00	100.00	100.00

Properties of TEPI based on DFT calculations

Quantum computing based on the DFT method allows us to support experimental conclusions. To do this, we started by determining the exact geometry of the evaluated inhibitor for its neutral (TEPI) and protonated (TEPI-H) forms, optimizing the geometry of each form without any geometric

restrictions, and identifying the frontier molecular orbital density distributions and other quantum chemical descriptors for each form.

Figure 10 shows the most stable configuration of the inhibitory molecule in its TEPI and TEPI-H forms. The distribution of HOMO and LUMO molecular orbitals and the electron density mapped with the iso-surface of the electrostatic potential (ESP) are shown in Figure 11. A closer analysis of HOMO distribution shows that it has a total localization of electron density at surface level. This suggests a high electron-donating capacity due to many local sites favoring the adsorption of this molecule to the metal surface in question. However, the LUMO distribution takes place at the level of an ethoxyphenyl structure, and the dihydro-imidazole of the molecule studied shows that these two parts are ready to receive electrons. These HOMO and LUMO distribution properties may lead to parallel adsorption with the Fe(110) metal support. This observation is well illustrated by the calculation of the electron density mapped with the iso-surface of the electrostatic potential (ESP) (Figure 11). The potential areas, both positive and negative, are represented by the colors red and blue, respectively. Oxygen and the non-protonated nitrogen atoms are the sites most vulnerable to electrophilic attack, further promoting adsorption power on the metal surface.

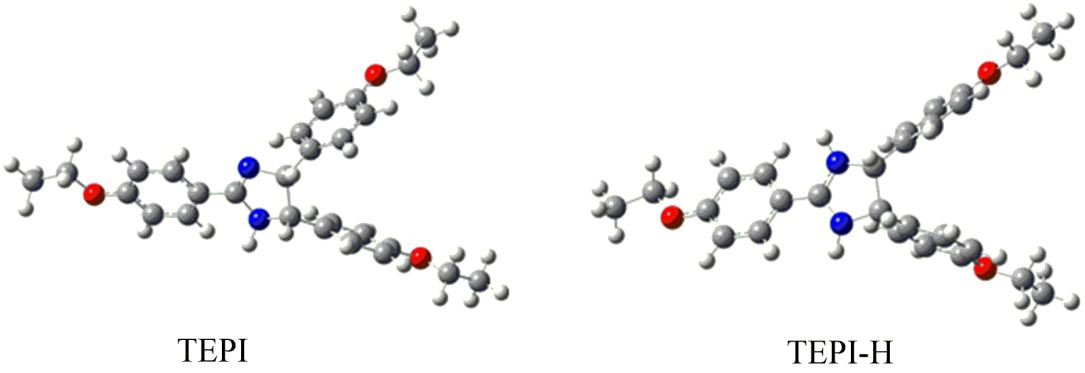

Figure 10. *Optimized geometry of TEPI and TEPI-H B3LYP/6-31G(d,p) in aqueous medium*

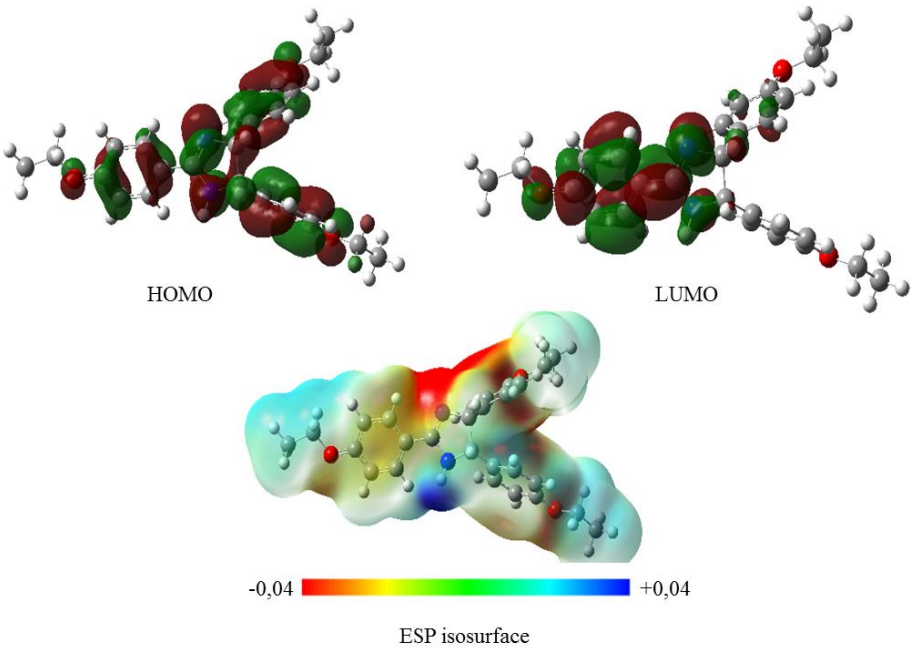

Figure 11*. HOMO and LUMO electron distributions and the electrostatic potential (ESP) of TEPI in aqueous medium*

The values of the calculated descriptors are presented in Table 8.

Table 8. *Calculated values of quantum chemical descriptors of TEPI in aqueous medium generated from the B3LYP/6-31G(d,p) level*

Compound	E_{HOMO} / eV	E_{LUMO} / eV	ΔE / eV	χ / eV	η / eV	ΔN	A / a.u.	μ / D
TEPI	-5.706	-0.810	4.897	3.258	2.448	0.319	413.496	3.173
TEPI-H	-6.152	-1.965	4.186	4.059	2.093	0.182	417.187	7.955

The HOMO (LUMO) energy value is associated with the electron-donating (accepting) ability of the corrosion inhibitor [42]. The high energy value of the HOMO indicates that it is easier for the TEPI to donate electrons to empty d orbitals in metals, which facilitates good adsorption and increases the value of corrosion inhibition efficiency.

In general, a low value of (ΔE) signifies that the molecule strongly interacts with the metal surface and acts as an effective corrosion inhibitor [43]. While it is difficult to discuss this parameter without comparing it with that of a similar compound, it is important to note that the energy gap of the TEPI in neutral and protonated forms is low (Table 8), especially in the protonated form, compared to numerous of mentioned corrosion inhibitors [43,44]. This observation confirms that the TEPI can easily adsorb on the metal surface, causing higher protection. The calculated global reactivity descriptors show that this molecule has a high nucleophilic power. This is consistent with the value of the calculated electron transfer index (0.319 and 0.182 for TEPI and TEPI-H, respectively), which, according to Koopmans, improves corrosion inhibition effectiveness [45]. The high values of the dipole moment and the polarizability of the proposed molecule (the dipole moment and the polarizability for the neutral form are 3.173 D and 413.496 a.u, respectively, and are 7.955 and 417.187 D for the protonated form) are also in agreement with this conclusion.

The calculated quantum descriptors show high structural chemical reactivity for both forms, with high inhibitory efficacy, which was experimentally proven.

Monte Carlo and molecular dynamic simulation results

To evaluate the properties of the proposed TEPI molecule as a corrosion inhibitor and to show its behavior with respect to the metallic surface, Monte Carlo (MC) and molecular dynamic (MD) simulations were performed. The objective of this simulation was to determine the lowest adsorption energy of our molecule when it is in contact with the iron surface by looking for its spontaneous configuration both in a vacuum and in an aqueous medium and finding its binding and interaction energy.

Recall that the binding and interaction energies are calculated from the energy of the total energy of the entire system (E_{Total}), the energy of the inhibitor ($E_{Inhibitor}$), and the energy of the Fe (110) surface ($E_{Surface}$) according to equations (9) AND (10).

$$E_{Interaction} = E_{Total} - E_{Inhibitor} - E_{Surface} \quad (9)$$

$$E_{Interaction} = E_{Binding} \quad (10)$$

Figure 12 shows the adsorption configuration of the TEPI inhibitor molecule on the metal surface, with the structural arrangement leading to the most stable adsorption energy. The energy results of this simulation, performed in aqueous medium, are summarized in Table 9.

The results of this study suggest that the proposed molecule can be a good corrosion inhibitor for steel since it has a high affinity towards the metallic surface. Its mode of adsorption is parallel and nearby, with significant adsorption energies in both phases. This adsorption energy becomes very high even in a corrosive medium (presence of H_2O, H_3O^+ and Cl^-), which indicates an easy and stronger interaction between the TEPI organic molecule and steel.

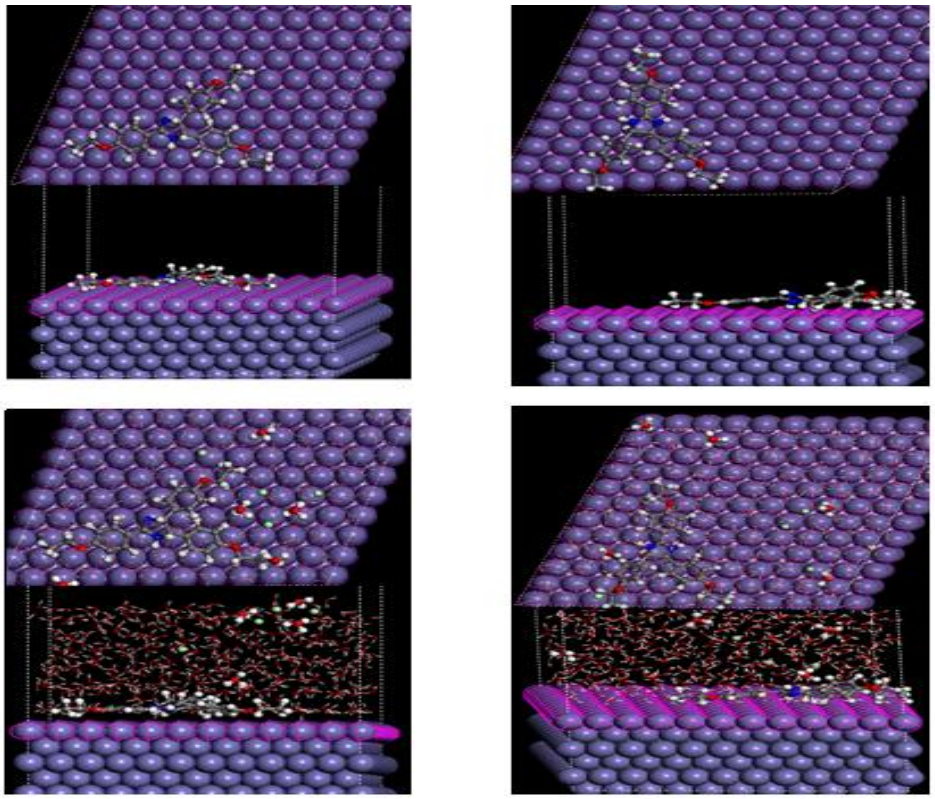

Figure 12. *Top and side views of the equilibrium adsorption geometries of TEPI and TEPI-H on the Fe (110) surface in aqueous medium*

Table 9. *The output energies calculated by MC simulation for adsorption of the studied inhibitor on Fe (110) surface in vacuum and aqueous medium*

Compounds	Energy, J mol^{-1}						
	Total	Adsorption	Rigid adsorption	Deformation	dE_{ad} / dN_i*		
					H_2O	H_3O	Cl
TEPI	-7305.074	-7497.324	-7692.210	194.886	-13.049	-148.616	-149.802
TEPI-H	-7342.728	-7534.977	-7728.602	193.624	-14.329	-147.804	-155.079

*dE_{ads} - change in adsorption energy, dN_i - change in the quantity of molecules adsorbed

Table 10. *MD simulation of TEPI and TEPI-H onto a Fe (110) surface at 303 K yielded interaction and binding energies*

Compound	$E_{Interaction}$ / kJ mol^{-1}	$E_{Binding}$ / kJ mol^{-1}
TEPI	1113.656	-1113.656
TEPI-H	1258.035	-1258.035

TEPI can adsorb efficiently on the metal surface in its neutral or protonated form thanks to the oxygen and nitrogen atoms of the imidazole ring and the phenyl rings. The presence of the oxygen atoms strengthens the polarity of the tails (ethoxyphenyl) of the molecule, which allows effective coverage of the surface and improves its inhibition properties.

To confirm these results and predict the binding energy, a molecular dynamic simulation was performed, and the equilibrium of the system was evaluated and confirmed by the stable average values of the energy fluctuations, taking into account the temperature factor (at experimental temperature 303 K). This simulation showed that the molecule can efficiently adsorb onto the surface while maintaining its orientation. The data in Table 10 also indicate that the binding energies

of the molecule with the Fe surface are very high and positive, suggesting a high stability of the adsorbed molecule [46,47].

The results of the MD and MC simulations show high adsorption of the two forms studied on Fe (110), which indicates that the inhibitor studied is highly effective against the corrosion phenomenon, as was already reported in the experimental section.

Corrosion inhibition mechanism

PDP findings confirmed the mixed nature of TEPI adsorption with the predominant cathodic type. Furthermore, the values of adsorption and thermodynamics parameters show that adsorption processes are both chemically and physically based. Therefore, the mechanism of corrosion inhibition could be explained by the adsorption process of the inhibitor onto the metal surface. It is reasonable to assume that TEPI molecules in the HCl medium may exist in the protonated form in equilibrium with the equivalent neutral molecular form according to:

$$TEPI + xH^+ \leftrightarrow (TEPIH)^{x+} \quad (11)$$

At first, a significant number of Cl^- ions from the HCl medium was adsorbed onto the positively charged C35E surface, creating a negative charge region. Subsequently, the protonated $(TEPIH)^+$ would be electrostatically adsorbed (physisorption) on this newly generated negatively charged surface, forming a protective film $(FeCl^-TEPIH^+)_{ads}$ and thus preventing the anodic corrosion reaction. Similarly, the cathodic reaction mechanism can be described as follows:

$$Fe + H^+ \rightarrow (FeH^+)_{ads} \quad (12)$$

$$(FeH^+)_{ads} + e^- \rightarrow (FeH)_{ads} + H^+ + e^- \rightarrow Fe + H_2\uparrow \quad (13)$$

The protonated $(TEPIH)^+$ ions were also adsorbed in the cathodic sites, where they compete with H^+ for electrons, reducing the production of H_2.

In addition to physisorption, chemisorption can occur by the displacement of pre-adsorbed water molecules from the C35E /aqueous medium interface. The O atoms (ethoxy) and/or N atoms of the imidazole ring might establish coordination bonds with the vacant d-orbital of iron atoms using their free electron pairs. Furthermore, the excess negative charge collected on the C35E surface can be transferred from the iron d-orbital to the empty π* orbital of TEPI molecules (retro-donation) (Figure 13), boosting TEPI adsorption on the C35E surface. Finally, the adsorbed inhibitor layer was formed on the C35E surface, acting as a barrier between C35E and 1 M HCl medium and preventing acid corrosion of C35E steel.

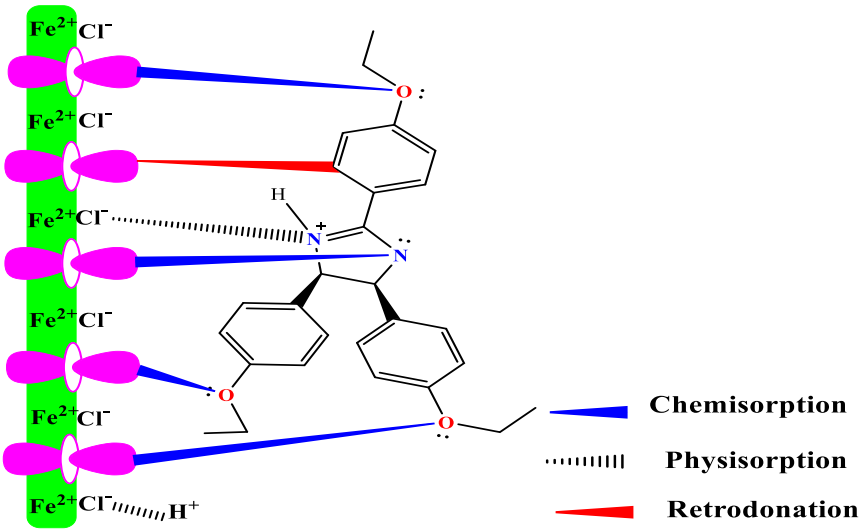

Figure 13. *Possible adsorption mechanism of TEPI on C35E steel surface in HCl medium*

Conclusion

The findings of this investigation reveal that TEPI is a good inhibitor of C35E steel corrosion in 1 M HCl at 303 K. It has been encountered that when the amount of TEPI rises, the effectiveness values for inhibition rise noticeably, achieving about 97 % in 1 mM HCl. According to the findings of PDP, TEPI is functioning as a mixed-type inhibitor. Adsorption of TEPI on the C35E steel surface in 1 M HCl rules the Langmuir adsorption isotherm model. Both SEM and UV-vis confirm that TEPI has an adsorption action on the surface of the C35E. In the same way, the calculated quantum descriptors show high structural chemical reactivity for both forms, with high inhibitory efficacy as experimentally proven. The results of the MD and MC simulations show strong adsorption of the two forms studied on Fe (110), providing better protection for the steel in question.

References

[1] D. H. Xia, C. Deng, D. Macdonald, S. Jamali, D. Mills, J.-L. Luo, M.G. Strebl, M. Amiri, W. Jin, S. Song, Electrochemical measurements used for assessment of corrosion and protection of metallic materials in the field: A critical review, *Journal of Materials Science & Technology* **112** (2021) 151-183. https://doi.org/10.1016/j.jmst.2021.11.004

[2] H. Wei, B. Heidarshenas, L. Zhou, G. Hussain, Q. Li, K. K. Ostrikov, Green inhibitors for steel corrosion in acidic environment: state of art, *Materials Today Sustainability* **10** (2020) 100044. https://doi.org/10.1016/j.mtsust.2020.100044

[3] R. Rodrigues, S. Gaboreau, J. Gance, I. Ignatiadis, S. Betelu, Reinforced concrete structures: A review of corrosion mechanisms and advances in electrical methods for corrosion monitoring, *Construction and Building Materials* **269** (2021) 121240. https://doi.org/10.1016/j.conbuildmat.2020.121240

[4] L. Xiong, P. Wang, Z. He, Q. Chen, J. Pu, R. Zhang, Corrosion behaviors of Q235 carbon steel under imidazoline derivatives as corrosion inhibitors: Experimental and computational investigations, *Arabian Journal of Chemistry* **14** (2021) 102952. https://doi.org/10.1016/j.arabjc.2020.102952

[5] P. Ren, J. Li, L. Wang, H. Guo, B. Lei, Z. Feng, G. Meng, Organo-Cerium as a Quick Repair Agent for Coating Damage on Carbon Steel, *Journal of Materials Engineering and Performance* **32** (2023) 9755-9764. https://doi.org/10.1007/s11665-023-07815-7

[6] S. Chen, Z. Huang, M. Yuan, G. Huang, H. Guo, G. Meng, Z. Feng, P. Zhang, Trigger and response mechanisms for controlled release of corrosion inhibitors from micro/nanocontainers interpreted using endogenous and exogenous stimuli: A review, *Journal of Materials Science & Technology* **125** (2022) 67-80. https://doi.org/10.1016/j.jmst.2022.02.037

[7] M. Benabdellah, R. Touzani, A. Aouniti, A. Dafali, S. El Kadiri, B. Hammouti, M. Benkaddour, Inhibitive action of some bipyrazolic compounds on the corrosion of steel in 1 M HCl: Part I: Electrochemical study, *Materials Chemistry and Physics* **105** (2007) 373-379. https://doi.org/10.1016/j.matchemphys.2007.05.001

[8] N. Chafai, S. Chafaa, K. Benbouguerra, D. Daoud, A. Hellal, M. Mehri, Synthesis, characterization and the inhibition activity of a new α-aminophosphonic derivative on the corrosion of XC48 carbon steel in 0.5 M H_2SO_4: experimental and theoretical studies, *Journal of the Taiwan Institute of Chemical Engineers* **70** (2017) 331-344. https://doi.org/10.1016/j.jtice.2016.10.026

[9] M. El Faydy, B. Lakhrissi, C. Jama, A. Zarrouk, L. O. Olasunkanmi, E. E. Ebenso, F. Bentiss, Electrochemical, surface and computational studies on the inhibition performance of some newly synthesized 8-hydroxyquinoline derivatives containing benzimidazole moiety against

the corrosion of carbon steel in phosphoric acid environment*, Journal of Materials Research and Technology* **9** (2020) 727-748. https://doi.org/10.1016/j.jmrt.2019.11.014

[10] M. Belayachi, H. Serrar, H. Zarrok, A. El Assyry, A. Zarrouk, H. Oudda, S. Boukhris, B. Hammouti, Eno E. Ebenso, A. Geunbour, New pyrimidothiazine Derivative as Corrosion Inhibitor for Carbon Steel in Acidic Media, *International Journal of Electrochemical Science* **10** (2015) 3010-3025. http://www.electrochemsci.org/papers/vol10/100403010.pdf

[11] H. Bendaha, A. Zarrouk, A. Aouniti, B. Hammouti, S. El Kadiri, R. Salghi, R. Touzani, Adsorption and corrosion inhibitive properties of some tripodal pyrazolic compounds on mild steelin hydrochloric acid systems, *Physical and Chemical News* **64** (2012) 95-103. https://www.researchgate.net/publication/263422004_Adsorption_and_corrosion_inhibitive_properties_of_some_tripodal_pyrazolic_compounds_on_mild_steel_in_hydrochloric_acid_systems

[12] H. Zarrok, R. Salghi, A. Zarrouk, B. Hammouti, H. Oudda, Lh. Bazzi, L. Bammou, S.S. Al-Deyab, Investigation of the Inhibition Effect of N-1-Naphthylethylenediamine Dihydrochloride Monomethanolate on the C38 Steel Corrosion in 0.5 M H_2SO_4, *Der Pharma Chemica* **4(1)** (2012) 407-416. https://www.derpharmachemica.com/pharma-chemica/investigation-of-the-inhibition-effect-of-n1naphthylethylenediamine-dihydrochloride-monomethanolate-on-the-c38-steel-cor.pdf

[13] B. Narasimhan, D. Sharma, P. Kumar, Biological importance of imidazole nucleus in the new millennium, *Medicinal Chemistry Research* **20** (2011) 1119-1140. https://doi.org/10.1007/s00044-010-9472-5

[14] L. Zhang, X. Peng, G.L. V Damu, R. Geng, C. Zhou, Comprehensive review in current developments of imidazole-based medicinal chemistry, *Medicinal Research Reviews* **34** (2014) 340-437. https://doi.org/10.1002/med.21290

[15] A. Khormali, S. Ahmadi, Synergistic effect between oleic imidazoline and 2-mercaptobenzimidazole for increasing the corrosion inhibition performance in carbon steel samples, *Iranian Journal of Chemistry and Chemical Engineering* **42** (2023) 321-336. https://doi.org/10.30492/ijcce.2022.546098.5091

[16] C. Zhang, J. Hu, Z. Yang, Z. Zheng, S. Geng, X. Zhong, Effects of the number of imidazoline ring and the length of alkyl group chain of imidazoline derivatives on corrosion inhibition of carbon steel in HCl solution: Molecular simulation and experimental validation, *Petroleum* **4** (2021) 447-457. https://doi.org/10.1016/j.petlm.2021.03.002

[17] G. Laadam, M. El Faydy, F. Benhiba, A. Titi, H. Amegroud, Arej S Al-Gorair, H. Hawsawi, R. Touzani, I. Warad, A. Bellaouchou, A. Guenbour, M. Abdallah, A. Zarrouk, Outstanding anticorrosion performance of two pyrazole derivatives on carbon steel in acidic medium: Experimental and quantum-chemical examinations, *Journal of Molecular Liquids* **375** (2023) 121268. https://doi.org/10.1016/j.molliq.2023.121268

[18] F. Benhiba, Z. Benzekri, Y. Kerroum, N. Timoudan, R. Hsissou, A. Guenbour, M. Belfaquir, S. Boukhris, A. Bellaouchou, H. Oudda, A. Zarrouk, Assessment of inhibitory behavior of ethyl 5-cyano-4-(furan-2-yl)-2-methyl-6-oxo-1,4,5,6-tetrahydropyridine-3-carboxylate as a corrosion inhibitor for carbon steel in molar HCl: Theoretical approaches and experimental investigation, *Journal of the Indian Chemical Society* **100** (2023) 100916. https://doi.org/10.1016/j.jics.2023.100916

[19] F. Benhiba, N.K. Sebbar, H. Bourazmi, M.E. Belghiti, R. Hsissou, T. Hökelek, A. Bellaouchou, A. Guenbour, I. Warad, H. Oudda, A. Zarrouk, E.M. Essassi, Corrosion inhibition performance of 4-(prop-2-ynyl)-[1,4]-benzothiazin-3-one against mild steel in 1M HCl solution: Experimental and theoretical studies, *International Journal of Hydrogen Energy* **46 (51)** (2021) 25800-25818. https://doi.org/10.1016/j.ijhydene.2021.05.091

[20] M. Yadav, S. Kumar, R.R. Sinha, I. Bahadur, E.E. Ebenso, New pyrimidine derivatives as efficient organic inhibitors on mild steel corrosion in acidic medium: Electrochemical, SEM, EDX, AFM and DFT studies, *Journal of Molecular Liquids* **211** (2015) 135-145. https://doi.org/10.1016/j.molliq.2015.06.063

[21] M. J. Frisch, G. W. Trucks, H. B. Schlegel, G. E. Scuseria, M. A. Robb, J. R. Cheeseman, G. Scalmani, V. Barone, B. Mennucci, G. Petersson, Gaussian 09, Revision D. 01, Gaussian, Inc., Wallingford CT. http://www.gaussian.com

[22] A.H. Al Hamzi, H. Zarrok, A. Zarrouk, R. Salghi, The Role of Acridin-9(10*H*)-one in the Inhibition of Carbon Steel Corrosion : Thermodynamic, Electrochemical and DFT Studies, *International Journal of Electrochemical Science* **9** (2013) 2586-2605. https://doi.org/10.1016/S1452-3981(23)14334-3

[23] H. Fakhry, M. El Faydy, F. Benhiba, T. Laabaissi, M. Bouassiria, M. Allali, B. Lakhrissi, H. Oudda, A. Guenbour, I. Warad, A. Zarrouk, A newly synthesized quinoline derivative as corrosion inhibitor for mild steel in molar acid medium: Characterization (SEM/EDS), experimental and theoretical approach, *Colloids and Surfaces A: Physicochemical and Engineering Aspects* **610** (2021) 125746. https://doi.org/10.1016/j.colsurfa.2020.125746

[24] V. Barone, M. Cossi, Quantum calculation of molecular energies and energy gradients in solution by a conductor solvent model, *The Journal of Physical Chemistry A,* **102** (1998) 1995-2001. https://doi.org/10.1021/jp9716997

[25] M.E. Belghiti, Y. Karzazi, S. Tighadouini, A. Dafali, C. Jama, I. Warad, B. Hammouti, S. Radi, New hydrazine derivatives as corrosion for mild steel in phosphoric acid medium. Part B: Theoretical investigation, *Journal of Materials and Environmental Science* **7** (2016) 956-967.

[26] Q. Nuha, A. Wazzan, Journal of Industrial and Engineering Chemistry DFT calculations of thiosemicarbazide, arylisothiocynates, and 1-aryl-2,5-dithiohydrazodicarbonamides as corrosion inhibitors of copper in an aqueous chloride solution, *Journal of Industrial and Engineering Chemistry* **26** (2014) 291-308. https://doi.org/10.1016/j.jiec.2014.11.043

[27] C. Verma, J. Haque, E. E. Ebenso, M. A. Quraishi, Results in Physics Melamine derivatives as effective corrosion inhibitors for mild steel in acidic solution: Chemical, electrochemical, surface and DFT studies, *Results in Physics* **9** (2018) 100-112. https://doi.org/10.1016/j.rinp.2018.02.018

[28] A. Mishra, C. Verma, H. Lgaz, Synthesis, characterization and corrosion inhibition studies of N-phenyl-benzamides on the acidic corrosion of mild steel: Experimental and computational studies, *Journal of Molecular Liquids* **251** (2017) 317-332. https://doi.org/10.1016/j.molliq.2017.12.011

[29] M. El Faydy, F. Benhiba, Y. Kerroum, A. Guenbour, F. Bentiss, I. Warad, B. Lakhrissi, A. Zarrouk, Synthesis and anticorrosion characteristics of new 8-quinolinol analogs with amide-substituted on C35E steel in acidic medium: Experimental and computational ways, *Journal of Molecular Liquids* **325** (2021) 115224. https://doi.org/10.1016/j.molliq.2020.115224

[30] A. El yaktini, A. Lachiri, M. El Faydy, F. Benhiba, H. Zarrok, M. El Azzouzi, M. Zertoubi, M. Azzi, B. Lakhrissi, A. Zarrouk, Practical and Theoretical Study on the Inhibitory Inflences of New Azomethine Derivatives Containing 8-hydroxyquinoline Moiety for the Corrosion of Carbon Steel in 1 M HCl, *Oriental Journal of Chemistry* **34(6)** (2018) 3016-3029. https://doi.org/10.13005/ojc/340643

[31] M. Rbaa, P. Dohare, A. Berisha, O. Dagdag, L. Lakhrissi, M. Galai, B. Lakhrissi, M.E. Touhami, I. Warad, A. Zarrouk, New Epoxy sugar based glucose derivatives as eco friendly corrosion inhibitors for the carbon steel in 1.0 M HCl: Experimental and theoretical investigations, *Journal of Alloys and Compounds* **833** (2020) 154949. https://doi.org/10.1016/j.jallcom.2020.154949

[32] M. El Faydy, M. Galai, M.E. Touhami, I.B. Obot, B. Lakhrissi, A. Zarrouk, Anticorrosion potential of some 5-amino-8-hydroxyquinolines derivatives on carbon steel in hydrochloric acid solution: Gravimetric, electrochemical, surface morphological, UV-visible, DFT and Monte Carlo simulations, *Journal of Molecular Liquids* **248** (2017) 1014-1027. https://doi.org/10.1016/j.molliq.2017.10.125

[33] F. Bentiss, F. Gassama, D. Barbry, L. Gengembre, H. Vezin, M. Lagrenée, M. Traisnel, Enhanced corrosion resistance of mild steel in molar hydrochloric acid solution by 1,4-bis(2-pyridyl)-5H-pyridazino[4,5-b]indole: Electrochemical, theoretical and XPS studies, *Applied Surface Science* **252** (2006) 2684-2691. https://doi.org/10.1016/j.apsusc.2005.03.231

[34] E. Alibakhshi, M. Ramezanzadeh, G. Bahlakeh, B. Ramezanzadeh, M. Mahdavian, M. Motamedi, *Glycyrrhiza glabra* leaves extract as a green corrosion inhibitor for mild steel in 1 M hydrochloric acid solution: Experimental, molecular dynamics, Monte Carlo and quantum mechanics study, *Journal of Molecular Liquids* **255** (2018) 185-198. https://doi.org/10.1016/j.molliq.2018.01.144

[35] N. Anusuya, J. Saranya, P. Sounthari, A. Zarrouk, S. Chitra, Corrosion inhibition and adsorption behaviour of some bis-pyrimidine derivatives on mild steel in acidic medium, *Journal of Molecular Liquids* **225** (2017) 406-417. https://doi.org/10.1016/j.molliq.2016.11.015

[36] P. Muthukrishnan, B. Jeyaprabha, P. Prakash, Adsorption and corrosion inhibiting behavior of Lannea coromandelica leaf extract on mild steel corrosion, *Arabian Journal of Chemistry* **10** (2017) S2343-S2354. https://doi.org/10.1016/j.arabjc.2013.08.011

[37] P. R. Ammal, M. Prajila, A. Joseph, Effect of substitution and temperature on the corrosion inhibition properties of benzimidazole bearing 1 , 3 , 4-oxadiazoles for mild steel in sulphuric acid : Physicochemical and theoretical studies, *Journal of Environmental Chemical Engineering* **6** (2018) 1072-1085. https://doi.org/10.1016/j.jece.2018.01.031

[38] H. Zarrok, A. Zarrouk, R. Salghi, Y. Ramli, B. Hammouti, S.S. Al-Deyab, E.M. Essassi, H. Oudda, Adsorption and inhibition effect of 3-methyl-1-propargylquinoxalin-2 (1H)-one on carbon steel corrosion in hydrochloric acid, *International Journal of Electrochemical Science* **7** (2012) 8958-80973. https://doi.org/10.1016/S1452-3981(23)18044-8

[39] I.B. Obot, N.O. Obi-Egbedi, Adsorption properties and inhibition of mild steel corrosion in sulphuric acid solution by ketoconazole: Experimental and theoretical investigation, *Corrosion Science* **52** (2010) 198-204. https://doi.org/10.1016/j.corsci.2009.09.002

[40] L. Bai, L. J. Feng, H. Y. Wang, Y. Bin Lu, X. W. Lei, F. L. Bai, Comparison of the synergistic effect of counterions on the inhibition of mild steel corrosion in acid solution: Electrochemical, gravimetric and thermodynamic studies, *RSC Advances* **5** (2015) 4716-4726. https://doi.org/10.1039/c4ra12286k

[41] A. Sedik, D. Lerari, A. Salci, S. Athmani, K. Bachari, İ. H. Gecibesler, R. Solmaz, Dardagan Fruit extract as eco-friendly corrosion inhibitor for mild steel in 1 M HCl: Electrochemical and surface morphological studies, *Journal of the Taiwan Institute of Chemical Engineers* **107** (2020) 189-200. https://doi.org/10.1016/j.jtice.2019.12.006

[42] I. Lukovits, I. Bakó, A. Shaban, E. Kálmán, Polynomial model of the inhibition mechanism of thiourea derivatives, *Electrochimica Acta* **43** (1998) 131-136. https://doi.org/10.1016/S0013-4686(97)00241-7

[43] D. Kumar, V. Jain, B. Rai, Imidazole derivatives as corrosion inhibitors for copper: A DFT and reactive force field study, *Corrosion Science* **171** (2020) 108724. https://doi.org/10.1016/j.corsci.2020.108724

[44] M. Li, Y. Ouyang, W. Yang, Y. Chen, K. Zhang, Z. Zuo, X. Yin, Y. Liu, Inhibition performances of imidazole derivatives with increasing fluorine atom contents in anions against carbon

steel corrosion in 1 M HCl, *Journal of Molecular Liquids* **322** (2021) 114535. https://doi.org/10.1016/j.molliq.2020.114535

[45] T. Koopmans, Ordering of wave functions and eigenenergies to the individual electrons of an atom, *Physic*a **1** (1933) 104-113. https://doi.org/10.1016/S0031-8914(34)90011-2

[46] M. Goyal, H. Vashisht, A. Kumar, S. Kumar, I. Bahadur, F. Benhiba, A. Zarrouk, Isopentyltriphenylphosphonium bromideionic liquid as a newly effective corrosion inhibitor on metal-electrolyte interface in acidic medium: Experimental, surface morphological (SEM-EDX & AFM) and computational analysis, *Journal of Molecular Liquids* **316** (2020) 113838. https://doi.org/10.1016/j.molliq.2020.113838

[47] A. Attou, M. Tourabi, A. Benikdes, O. Benali, H. B. Ouici, F. Benhiba, A. Zarrouk, C. Jama, F. Bentiss, Experimental studies and computational exploration on the 2-amino-5-(2-methoxyphenyl)-1,3,4-thiadiazole as novel corrosion inhibitor for mild steel in acidic environment*, Colloids and Surfaces A* **604** (2020) 125320. https://doi.org/10.1016/j.colsurfa.2020.125320